The Counterbend Phenomenon in Dynein-Disabled Rat Sperm Flagella and What It Reveals about the Interdoublet Elasticity

Charles B. Lindemann, Lisa J. Macauley, and Kathleen A. Lesich
Department of Biological Sciences, Oakland University, Rochester, Michigan 48309-4476

ABSTRACT Rat sperm that have been rendered passive by disabling the dynein motors with 50 μM sodium metavanadate and 0.1 mM ATP exhibit an interesting response to imposed bending. When the proximal flagellum is bent with a microprobe, the portion of the flagellum distal to the probe contact point develops a bend in the direction opposite the imposed bend. This "counterbend" is not compatible with a simple elastic beam. It can be satisfactorily explained by the sliding tubule model of flagellar structure but only if there are permanent elastic connections between the outer doublets of the axoneme. The elastic component that contributes the bending torque for the counterbend does not reset to a new equilibrium position after an imposed bend but returns the flagellum to a nearly straight or slightly curved final position after release from the probe. This suggests it is based on fixed, rather than mobile, attachments. It is also disrupted by elastase or trypsin digestion, confirming that it is dependent on a protein linkage. Adopting the assumption that the elasticity is attributed to the nexin links that repeat at 96 nm intervals, we find an apparent elasticity for each link that ranges from 1.6 to 10 $\times$ 10^{-5} N/m. However, the elasticity is nonlinear and does not follow Hooke's law but appears to decrease with increased stretch. In addition, the responsible elastic elements must be able to stretch to more than 10 times their resting length without breakage to account for the observed counterbend formation. Elasticity created by some type of protein unfolding may be the only viable explanation consistent with both the extreme capacity for extension and the nonlinear character of the restoring force that is observed.

INTRODUCTION

The eukaryotic flagellum is a complex biological machine that harnesses the action of thousands of dynein molecular motors to produce useful mechanical work in the form of flagellar beating. The dynein motors apply the force they generate to the scaffolding of doublet microtubules, radial spokes, and interdoublet linkages that are collectively called the axoneme. To develop a fuller understanding of the mechanism that allows the action of the dynein motors to be converted into waves of bending, it is necessary to build an accurate conception of the way the axoneme responds to applied force.

Some of the fundamental properties of the axoneme have already been established by careful investigation. Satir (1,2) first showed that the outer doublets slide past each other during the course of the ciliary beat of a fresh water mussel. This working principle was extended to sea urchin sperm flagella by Summers and Gibbons (3) who additionally showed that when the basal body was removed by sonication the doublets could undergo free sliding, if the axoneme was treated with trypsin. The free sliding experiments suggest that mechanical linkages between the doublets prevent free sliding in an intact axoneme.

The interdoublet linkages observed in transmission electron micrographs (TEM) are called the nexin links. From the free sliding studies it would appear obvious that the nexin links, or some other structure that is easily proteolyzed, prohibit free sliding between the doublets. However, the amount of interdoublet shear that develops in a flagellar beat can be quite large, and an interdoublet linkage would have to be able to accommodate the normal range of interdoublet sliding without breaking.

In a beating sea urchin sperm, the bend angles of each propagating bend can exceed 3 radians (4). This corresponds to a shear angle of $\pm$1.5 radians and an interdoublet sliding of over 100 nm. The resting nexin length is $\sim$30 nm as measured from TEM micrographs. This means that the nexin links must routinely stretch to at least three times their resting length. The best visual support suggesting that this may be possible is from the micrographs of disintegrated rat sperm shown by Linck (5). The micrograph in Fig. 4 of that report shows structures that seem to repeat at the right intervals to be nexin links and are shown stretching between two separating doublets.

Yagi and Kamiya (6) provided a direct measurement of the interdoublet elastic component in sea urchin sperm axonemes. Their experiments appear to confirm the presence of an interdoublet elastic resistance. If the elastic component they measured is attributed to the nexin links, it yields 2.0 $\times$ 10^{-5} N/m per link as an estimate of the nexin link elasticity.

Other evidence casts doubt on the simple, straight forward view that the nexin links are permanent elastic connections. Bozkurt and Woolley (7) presented evidence that the nexin are not fixed but may translocate as sliding occurs. Minoura et al. (8) used a calibrated glass microprobe to measure the force required to produce lateral displacement of an outer doublet in sections of *Chlamydomonas* axoneme. They found an interdoublet elasticity that varied in stepwise increments. This suggests that the responsible elastic elements could translocate. It is also puzzling that a nexin link gene(s)

Submitted February 4, 2005, and accepted for publication May 27, 2005.

Address reprint requests to Charles B. Lindemann, Tel.: 248-370-3576; Fax: 248-370-4225; E-mail: lindeman@oakland.edu.

0006-3495/05/08/1165/10 $2.00

doi: 10.1529/biophysj.105.060681

has not shown up in the extensive library of mutations in *Chlamydomonas*. These inconsistencies have left both the molecular and functional nature of the nexin links in a state of uncertainty.

In this study, we take a different approach to studying the mechanics of the axoneme by using the large flagellum of rat sperm. Recently, we conducted a study of the stiffness of rat sperm flagella. To obtain the passive stiffness of the flagellar structures without the influence of the dynein motors, we adapted a procedure from Gibbons and Mocz (9) to disable the dyneins with 50 μM $NaVO_3$. We manipulated the passive flagella with force-calibrated glass microprobes to measure the force and torque needed to bend the passive flagella. In the course of the study, we observed that the portion of the sperm flagella distal to the probe contact point always developed a bend in the opposite direction to the bend introduced by the microprobe on the proximal portion.

It occurred to us that this counterbend was a result of the interdoublet shear produced by bending the passive flagellum and that it could yield valuable insight into the mechanics of the passive flagellum. By taking advantage of this very clear-cut and tractable mechanical response, we are able to derive an independent measurement of the nexin link elasticity to compare to that of Yagi and Kamiya (6). Our measurements suggest that the elasticity is not linear ''Hooke's law'' behavior, but is more complex.

MATERIALS AND METHODS

Sperm preparation

Rat sperm from the cauda epididymis of sexually mature, CO_2-euthanized Sprague-Dawley rats (Harlan, Indianapolis, IN) were recovered in 4 ml of sodium citrate buffer (0.097 M sodium citrate, 2 mM fructose, and 5 mM magnesium sulfate, pH 7.4) to make a stock sperm suspension as explained in Schmitz-Lesich and Lindemann (10). All chemical reagents used in this study were from Sigma Chemical (St. Louis, MO) and of the highest purity available, unless stated otherwise.

Dynein inactivation

To induce a passive state, sperm cells were treated with 50 μM $NaVO_3$ and 0.1 mM ATP via a process that required two stages. The complete details are given in Schmitz-Lesich and Lindemann (10). Briefly, the extraction medium contained 0.45 M sodium acetate, 2.5 mM magnesium acetate, 0.5 mM EDTA, 50 μM $NaVO_3$, and 10 mM HEPES (pH = 7.4). First, the sperm were extracted by combining 0.5 ml of the extraction treatment medium with 0.6 μl of 10% Triton X-100 (Pierce, Rockford, IL) and 100 μl of the stock sperm suspension. Next, the final suspension was produced by combining 3 ml of extraction medium with 0.1 mM ATP (Fisher Scientific, Hanover Park, IL) and 60 μl of the extracted sperm suspension from the previous step. A 0.01 M stock solution of $NaVO_3$ was prepared on the day of the experiment to prevent the possibility of oxidation.

A volume of 1.35 ml of the final suspension was transferred to an acrylic chamber (1 × 3 cm opening) with a glass coverslip bottom. The bottom of the chamber was pretreated with 0.05 M KOH and 100% acetone, in succession, to assist in the adherence of sperm heads to the surface of the chamber. $NaVO_3$-treated sperm cells were viewed with phase contrast illumination on a Nikon (Melville, NY) TE 2000U inverted microscope. Sequences of individual experimental runs were captured as .avi files on a custom built Pentium IV computer using a JAI Pulnix (Sunnyvale, CA) 9710 camera and Matrox Imaging's Meteor II digital framegrabber and Inspector 4.0 software (Dorval, Quebec, Canada). All computerized measurements were done using Inspector 4.0 or 4.1.

Sperm manipulation

Sperm chosen for manipulation had no obvious gross defects, were adhered to the bottom of the chamber by their heads, and showed unobstructed movement of the flagellum. All experiments were done within 1 h of initiating the $NaVO_3$ treatment. Microprobes, made from 1-mm borosilicate glass rod (Sutter Instruments, Novato, CA), were used to induce a bend in $NaVO_3$-treated (passive) flagella with the movement of the microprobe controlled by Sutter Instrument's MP-285 micromanipulator. All experiments were performed on a Technical Manufacturing (Peabody, MA) MICRO-g vibration isolation table. To evaluate the progressive response of an individual cell to manipulation, multiple frames ($n = 4$) from a single experimental run were analyzed. Each of the images selected for analysis of the counterbend was carefully chosen such that the flagellum was clearly visible most, if not all, of its entire length, the point of microprobe contact with the flagellum was delineated, neither the probe nor the flagellum were obstructed, and a range of responses was represented.

Trypsin and elastase treatment

Rat sperm treated with $NaVO_3$ as above were exposed to trypsin or elastase following a method adapted from Shingyoji and Takahashi (11). The final suspension of $NaVO_3$-treated sperm was exposed to 6 μg/ml of soybean trypsin inhibitor before treatment with 25 μg/ml of elastase (porcine pancreatic Type III). After 5 min, enzyme activity was inhibited with 150 μg/ml ovoinhibitor (chicken egg white Type IV). For the trypsin treatment, the final suspension of $NaVO_3$ cells was exposed to 7 μg/ml of trypsin (bovine pancreatic) for 3 min before inhibition with 10 μg/ml soybean trypsin inhibitor.

Shear angle and curvature measurements

Images of rat sperm cells exhibiting counterbends were selected for visibility and represent a range of counterbend responses. Shear angles were measured at 10 μm intervals along the flagellum, with point of contact between the flagellum and microprobe designated as the zero position. To achieve this, an individual image of the bent flagellum was measured and marked at each 10 μm segment of the proximal and distal flagellum using Inspector 4.0, resized in PowerPoint to accurately reflect real world dimensions, and printed. The shear angles were determined by drawing a line tangent to the flagellum at each 10 μm point and measuring the intersection of each tangent line with a tangent line drawn through the flagellar base. Since the flagellum inserts into the sperm head in such a way that the relaxed straight flagellum is aligned with the concave surface of the sperm head, the sperm head was used as a guide to locate the basal axis of the flagellum. This was especially useful when the flagellum was highly curved near the base. The curvature of the counterbend was determined by matching a circle of known radius to the curve of the first 20 μm segment of the flagellum distal to the point of contact with the probe. The curvature of the best fit circle was taken as a close approximation of the curvature of the flagellum at a point 10 μm beyond the probe contact. The inverse of the radius of the circle (meters) equals the curvature in radians/m.

Estimation of interdoublet shear

In mammalian sperm the large outer dense fibers (ODFs) attached to the individual doublets convey force from the doublet microtubules to the connecting piece. In turn, the ODF spacing in the plane of the beat becomes

the main determinant for the development of interdoublet shear. To analyze the interdoublet shear that develops in response to bending in such a system, it is necessary to find an estimate of the ODF separation as a function of flagellar position. Several published reports on the ultrastructure of rat sperm were consulted to take measurements from TEMs of the ODF and interdoublet spacing at recognizable landmarks along the flagellum. The numbering system for the doublets and ODFs as applied to the mammalian sperm axoneme by Woolley (12) is used throughout.

An ideal basal section of the axoneme is found in Fig. 5 *b* of Woolley (13) where a portion of the sperm head is adjacent to the section, ensuring that the section is very close to the base and connecting piece. The section is cut at a slight angle to perpendicular, as the central microtubular axoneme has a 212 nm diameter in the 1 to 5–6 axis and a diameter of 176 nm in the 3 to 8 axis. Dividing the measured distances in the 1 to 5–6 axis by the 1.2 ratio of the two diameters was used to correct for the distortion. The figure yields center to center spacing of 526 nm for ODFs 1 and 5–6 and a center to center spacing of 390 nm for ODFs 7–9 and 2–4.

The dark field images of Fig. 1 *A* in Lindemann et al. (14) give an empirical way of estimating the ODF length in comparison to the total flagellar length. The extruded ODFs can be seen to taper in intensity to ~120 μm, and the flagellar length is ~175 μm as measured from the same images. This means that the last 55 μm of the axoneme has no ODFs and that the largest ODFs taper to zero diameter at a distance of ~120 μm.

A TEM micrograph in Calvin and Cooper (15) provided a second opportunity to check the ODF spacing at a known position. Fig. 3 in that report shows a cross section of a rat sperm axoneme sectioned so precisely at the midpiece-principal piece junction that both lateral columns of the fibrous sheath and ODFs 3 and 8 are all visible in the section. ODFs 3 and 8 end where the lateral columns commence; this places the position of the section at 66 μm along the flagellum, which is the midpiece-principal piece junction. The measurements from this source agreed with the 1 to 5–6 basal spacing but gave a better fit if the basal separation of the 7–9 and 2–4 ODF was reduced to 300 nm.

In the main part of the flagellum where ODFs are a factor, the ODF spacing decreases from a maximum at the flagellar base and becomes equal to the interdoublet distances at 120 μm along the flagellum. If we assume that the ODF taper is linear with distance, then the following expressions will approximate the 1 to 5–6 effective diameter and the 2–4 and 7–9 effective diameter:

$$D_{\text{eff}}(1, 5-6) = -2.88\,S + 526 \quad (1)$$

$$D_{\text{eff}}(2, 4) = -1.56\,S + 300. \quad (2)$$

These equations can be used to find a local inter-ODF spacing to find the shear between doublets 1 and 5–6 and doublets 2 and 4 at any position, *S*, up to 120 μm along the flagellum.

The center to center interdoublet spacing in a rat sperm axoneme was measured from a number of TEM micrographs in several sources (14–16) and is ~180 nm for the 1 to 5–6 spacing and 113 nm for the 2–4 and 7–9 spacings. These interdoublet distances are the relevant distances for calculating interdoublet shear in the distal portion of the flagellum that lacks ODFs. So in the distal 55 μm, the interdoublet distances which determine interdoublet shear are 57 nm (half of 113 nm total) for doublets 2, 3, and 4 and also for doublets 7, 8, and 9. The interdoublet distance that determines the shear between doublets 9, 1, and 2 and also 4, 5–6, and 7 are equal to half of the difference between the whole axoneme diameter and the 2 to 4 and 7 to 9 spacing (180 minus 113 divided by 2) or 34 nm.

Starting from the base of the flagellum, the change in shear angle over each marked interval was multiplied by the ODF spacing found from Eqs. 1 and 2 for the midpoint of the interval. Shear was accumulated as a running total down the flagellar length for the 1 to 5–6 doublets and for the doublets 2 to 4 (which is also the shear between doublets 7 and 9). The shear between every doublet pair in the axoneme can then be found by subdividing the total shear. As an example, if we find the total shear developed between doublets 1 and 5–6 (*A*) and the total shear between doublet 2 and 4 (*B*), then the shear between doublets 1 and 2 will be half of the difference of the two totals ((*A* − *B*)/2).

RESULTS

Observations of protease sensitive counterbends

When rat sperm are permeabilized with 0.01% Triton X-100 and treated with 50 μM $NaVO_3$ and 0.1 mM ATP, they exhibit no active responses and appear to be flaccid. This concentration of $NaVO_3$ is known to inhibit dynein and favors the relaxed conformation of the dynein cross-bridge (17–19). Rat sperm that were in this condition were stuck to a glass slide by their heads and were manipulated with a glass microprobe to impose a bend on the flagellum. When this was done, the portion of the flagellum distal to the probe contact point responded to the bending of the flagellum by developing a bend in the opposite direction, as shown in Fig. 1. As is seen in the figure, the counterbend response grows proportionately larger as the bend imposed by the microprobe is increased. The counterbend response was recorded and analyzed in detail for seven cells. Table 1 gives the imposed bending and measured counterbend responses for these seven cells.

From a mechanical standpoint, this counterbend response cannot be explained by the flexion of a simple elastic beam. However, it is compatible with the sliding doublet model of the flagellar axoneme first proposed by Satir (1,2) and put into a mathematical framework by Brokaw (20,21). If the sliding doublet model is used as a basis for understanding the counterbend, it can still only be explained if the sliding

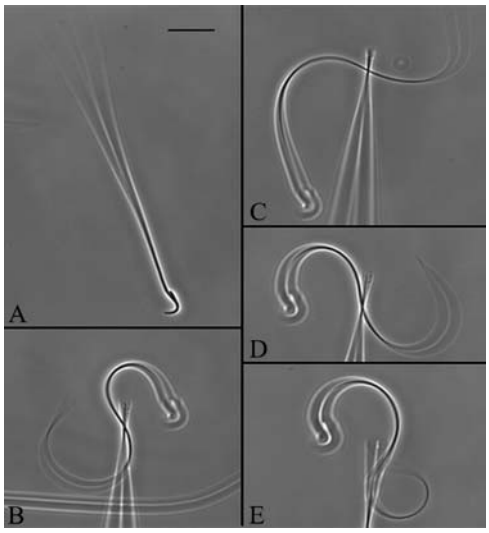

FIGURE 1 Counterbend formation in vanadate-inhibited rat sperm. The figure shows rat sperm that have been permeabilized with Triton X-100 and treated with 50 μM $NaVO_3$ in the presence of 0.1 mM ATP. The same cell is shown at equilibrium (*A*) and bent to varying degrees with a glass microprobe. (*B*) The flagellum is bent in the direction of the head curvature and exhibits a counterbend in the portion of the flagellum beyond the probe contact point. The counterbend is in the direction opposite to the imposed bend. (*C–E*) The flagellum is bent in the direction opposite to the curvature of the head. Note that the curvature of the counterbend varies in proportion to the imposed bending. Bar = 20 μm.

TABLE 1 Cells selected for numerical analysis

Cell	Probe position (μm)	Shear angle at probe (Radians)*	Shear angle at tip (Radians)*	Curvature (Radians/m $\times$ 10^4)
1	97	3.05	−0.99	6.8
2	29	1.27	−0.79	4.3
3†	72	3.51	−0.16	5.6
4	51	1.24	−0.75	2.2
5	86	2.34	−0.09	4.6
6	98	2.50	−1.20	6.3
7a	94	2.50	−1.13	5.9
7b	104	1.92	−0.93	4.8
7c	104	2.06	−0.17	3.9
7d	100	1.50	0.09	2.6

*A positive sign denotes a shear angle in the direction of the imposed bend.
†Cell analyzed with bend induced in the same direction as the natural curve of sperm head.

doublets have an elastic tendency to restore themselves to the zero-shear configuration by means of fixed elastic linkages that ''remember'' an invariant zero-shear position. If we assume that interdoublet linkages are responsible for the development of the counterbend, then the proteolytic agents used to induce free-sliding of the doublets in axoneme flagellar fragments should reduce or eliminate the response. We found that both trypsin and elastase digestion eliminated counterbend formation. Elastase is reported to be the more specific of the two agents in damaging nexin links with less damage to spokes and dyneins (11,22,23). Fig. 2 shows that elastase can completely eliminate the counterbend response when applied at 25 μg/ml for 5 min.

Interdoublet shear in the counterbend

In Brokaw's analysis of interdoublet shear, he showed that the sliding of one doublet relative to another is found by multiplying the local shear angle by the doublet separation (24). The local shear angle is the angle of the flagellar shaft at the point under consideration minus the angle of the flagellar shaft at the fixed basal anchor. The appropriate separation distance between the doublets is the center to center separation measured in the plane of bending. The bending plane is normally perpendicular to the axis of the central pair (25). The counterbend response was examined with respect to the shear angle induced at the probe contact point and the shear angle at the most distal portion of the flagellum, as illustrated in Fig. 3.

The second thing that can be seen both qualitatively in Fig. 1 and quantitatively in the graphic analysis in Fig. 3 is that the counterbend can develop a shear angle near the flagellar tip that exceeds the shear angle introduced by the microprobe. As shown in Fig. 3 *A*, the plotted shear angle data for

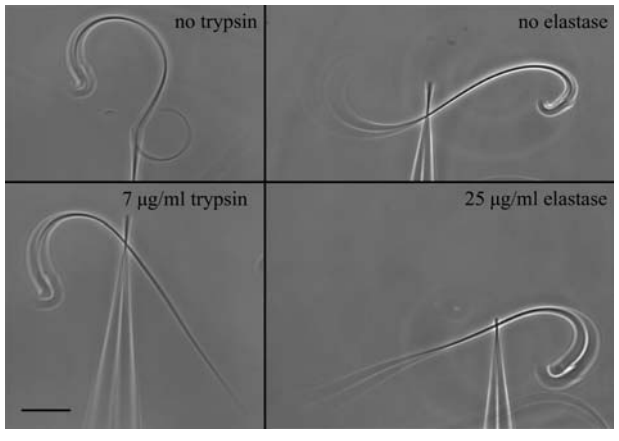

FIGURE 2 Elimination of the counterbend response with trypsin and elastase. The upper panels show 50 μM $NaVO_3$-treated rat sperm flagella manipulated to produce typical counterbend responses. The lower panels show the same cells manipulated into approximately the same proximal bend after treatment with 7 μg/ml trypsin for 3 min (*lower left*) and 25 μg/ml elastase for 5 min (*lower right*). Note the absence of the counterbends. Bar = 20 μm.

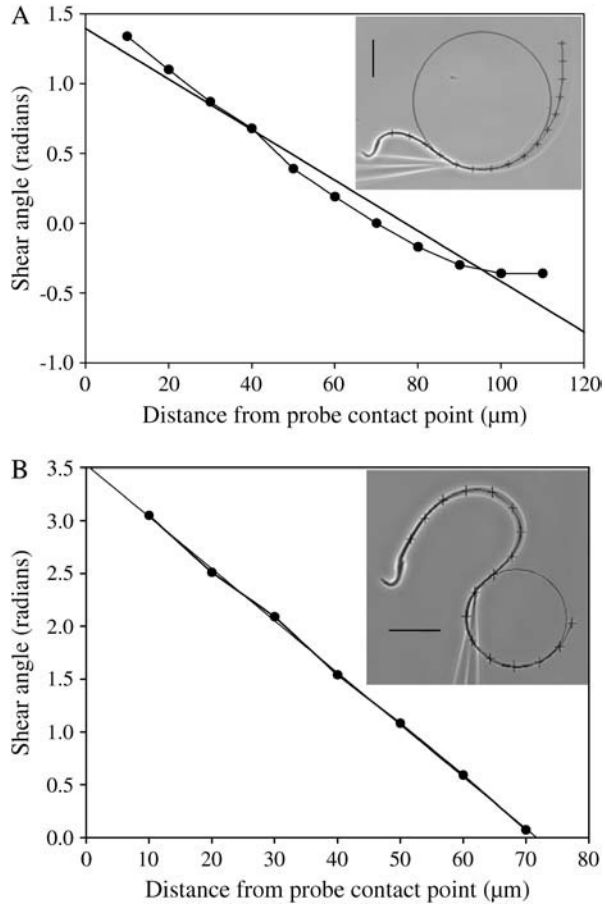

FIGURE 3 Shear angles in the counterbend. The shear angles in two counterbends are displayed for a cell bent to a shear angle of ~1.4 radians (*A*) and for a cell bent to ~3.1 radians (*B*). The cell that the data were taken from is shown as an inset in each graph. The inset also shows the circle used to match the curvature of the 20 μm segment adjacent to the probe for the analysis of the elastic torque. Notice that the flagellum in *A* exhibits a shear angle at the flagellar tip that is negative, more than reversing the shear introduced by the probe. Also note that the more severely bent cell in *B* exhibits a nearly circular counterbend and this is reflected in a linear shear angle plot. Bar = 20 μm.

the counterbend becomes negative near the flagellar tip. This relationship of the shear angle is relatively consistent. Table 1 gives the shear angles at the flagellar tip of seven cells in different degrees of imposed bending. The shear angle is negative, indicating an excess shear response at the flagellar tip greater than the imposed shear angle in all but one case. The single exception is the least bent configuration of cell No. 7, a cell that exhibited a shear excess in three more sharply bent configurations. Since the interdoublet spacing is uniform along the entire flagellum, the interdoublet shear in the counterbend of the distal flagellum should be limited to no more than the interdoublet shear in the proximal flagellum. The explanation that is most compatible with the observed behavior is that in a rat sperm, bending of the proximal region of the flagellum generates more interdoublet sliding than is predicted by the interdoublet spacing.

In the Geometric Clutch computer model developed for bull sperm (26), it was noted that mammalian sperm flagella have a peculiarity that potentially affects the way the doublets develop shear. The ODFs of these flagella attach to the outer doublets along most of the flagellar length and therefore slide as the doublets slide (14,16,27). The basal body disappears early in sperm development (28), leaving the doublets and the ODFs mechanically connected to the base of the flagellum by the structure called the connecting piece. Consequently, when dynein pulls on the outer doublets the tension generated on the outer doublets is communicated to the base of the flagellum through the ODFs to the connecting piece. This arrangement is illustrated in Fig. 4. The separation of the ODFs in the proximal portion of a rat sperm flagellum is much larger than the interdoublet spacing. In constructing a computer model of the bull sperm axoneme (26), it was hypothesized that the ODF spacing is the determinant of shear displacement, and this allowed simulation of the bull sperm beat.

The deduction that the ODF spacing should determine shear displacement in mammalian sperm was built into the Geometric Clutch model for bull sperm but, to our knowledge, until now it was not verified experimentally. The shear angles in the counterbend appear to support the view that the ODFs amplify shear development in the mammalian sperm axoneme. The view of axoneme mechanics illustrated in Fig. 4 was used as the basis for analyzing the counterbend response of rat sperm.

Seven cells were analyzed using the procedure described in Materials and Methods. There was always sufficient shear generated in the proximal flagellum to account for the recoil shear in the distal counterbend, using the values for interdoublet shear calculated with the ODF spacings found from Eqs. 1 and 2. In two instances this was barely the case, with zero shear being present near the end of the flagellum. This would argue that the equations are either just about right or are yielding a slight underestimate of the proximal shear. Intuition says there should be a little leftover shear, as elastic restoring force should not be able to attain a perfect

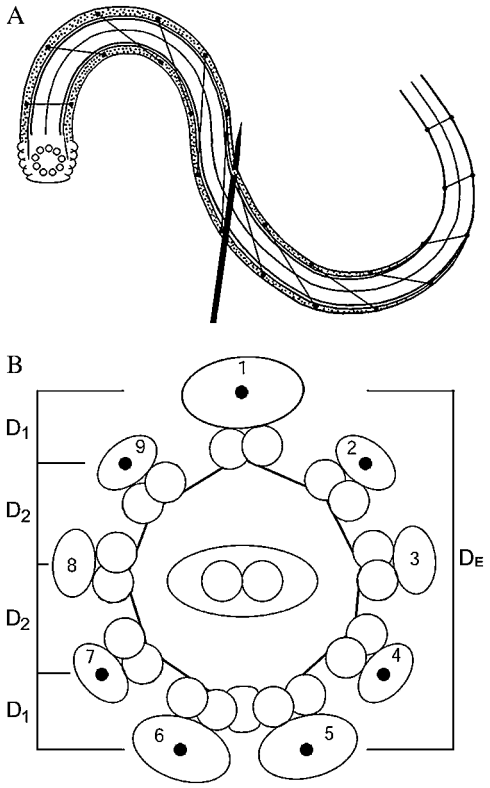

FIGURE 4 A schematic diagram of the mechanism of interdoublet shear formation in rat sperm. The outer doublets of mammalian sperm are connected along their length to the ODFs. These are in turn anchored at the flagellar base in a structure called the connecting piece. This is schematically illustrated in *A*. When the flagellum is bent, the spacing between the ODFs in the plane of the bend, as illustrated in *B*, is the spacing that governs the amount of shear that develops between the doublets. This accumulation of shear is illustrated in *A* by marking points along the ODFs at equal distances from the base and connecting them with straight lines. Shear introduced in the proximal flagellum by the probe causes interdoublet sliding in the counterbend region as shown in *A*. This sliding results in stretch of the interdoublet linkages (nexin links), which in turn generates the internal torque that maintains the shape of the counterbend.

restoration of zero shear. If the ODFs did not amplify interdoublet shear, the amount of shear we observe in rat sperm counterbends could not be supported.

Shape and symmetry of counterbends

We observed that as the amount of imposed bending is increased and the shear angle at the probe position increases, the counterbend becomes progressively more circular. This is evident in the comparison provided between Fig. 3, *A* and *B*. It is also found in the progression of imposed bends measured on a single cell and displayed in Fig. 5. The counterbends tended to become circular beyond a curvature of 4×10^4 radians/m. We noticed this because the plots of shear angle versus flagellar position are almost perfect straight lines for these cells, as shown in Figs. 3 *B* and 5 *A*. The cells with a linear change in shear angle thus provided an independent way to verify the curvature values used in the analysis.

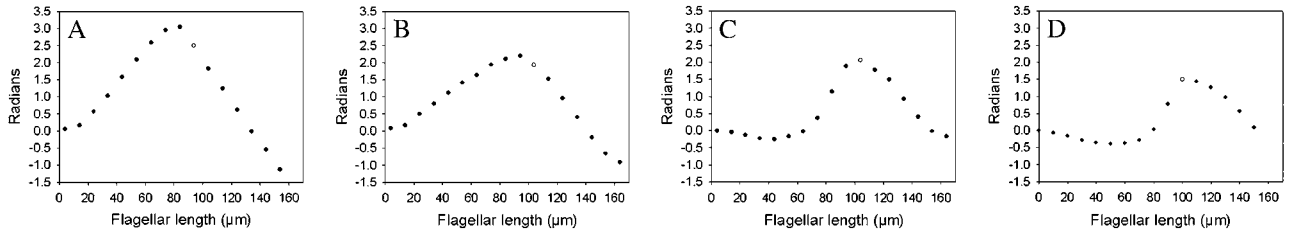

FIGURE 5 Shear angle profiles in the counterbend response. The shear angles from base to tip are plotted against flagellar position for the four positions of cell No. 7 (see Table 1) that were analyzed in this study. The position of the microprobe contact is indicated by the open circle. The four panels *A–D* correspond to the temporal order as the cell was progressively moved to a less bent configuration with the microprobe.

The fibrous sheath and the stiffness of the flagellum both decrease in size from the base to the tip. It is therefore quite interesting that the restoring force provided by the interdoublet linkages must also diminish in the exact same proportion; otherwise the curvature would not be circular.

All but one of the cells analyzed in this study were bent in the direction opposite to the natural curve of the sperm head; the exception was cell No. 3. We consistently noted that cells bent in the same direction as the natural curve of the sperm head seemed to show a weaker counterbend response for the same induced shear angle than those bent in the direction opposite to the head curvature. There was also a tendency for the released flagellum to retain residual curvature when bent in the same direction as the head curve and less of a tendency to retain curvature from being bent in the opposite direction.

These results hint that there is some asymmetry in the structure and mechanics of mammalian sperm flagella. The shear developed in the distal flagellum is not identical when the flagellum is bent in the two opposing bending directions. The counterbend is tighter, indicating more shear is present, when the induced bend is in the opposite direction of the head curvature as can be seen in Fig. 1. This is the same direction as the bend induced by the Ca^{2+} (fishhook) response in rat sperm. A plausible explanation for this discrepancy is if some of the shear created when the flagellum is bent in the direction of the head curvature is absorbed by an elastic deformation of the connecting piece. Vernon and Woolley (29) proposed such a mechanism, based on doublet displacements measured at the flagellar tip. Our evidence can be viewed as further support for this interpretation.

Interdoublet elasticity

A surprising finding from our shear analysis on cells in a counterbend is that the amount of interdoublet sliding is often very large. In the high shear area near the probe, cell 1 had 350 nm of sliding displacement between doublets 2 and 3, 3 and 4, 7 and 8, and 8 and 9. This cell appeared to suffer no permanent damage from the bending and recovered most of the way to its relaxed position when released. The nexin length is difficult to measure directly, but from the TEM images in Olson and Linck (16) we obtained an average of 30 nm for the most visible links in two high quality, high magnification images of the rat sperm axoneme. This rest length would require the nexin links to stretch to 12 times their resting length without breaking!

Restoring force and nexin link elasticity

The counterbend response can be used to glean some additional quantitative information about the restoring force that generates the bending. The passive flagellar stiffness is the key information needed to quantitate the magnitude of the restoring force. Recently, we accumulated a significant amount of data on the stiffness of dynein-disabled rat sperm flagella under the same working conditions used in this study (10); the data are shown in Fig. 6.

Ideally, the torque that must be applied to create a bend is a product of the curvature and the stiffness. In our earlier study we confirmed that rat sperm flagella show a linear relationship of torque to curvature, but there is an offset, or dead zone, of $\sim 1 \times 10^4$ radian/m which does not generate an elastic restoring force (see Fig. 5 of Schmitz-Lesich and Lindemann (10)). Therefore, for the purposes of this study, using the apparent stiffness from Fig. 6 could overestimate

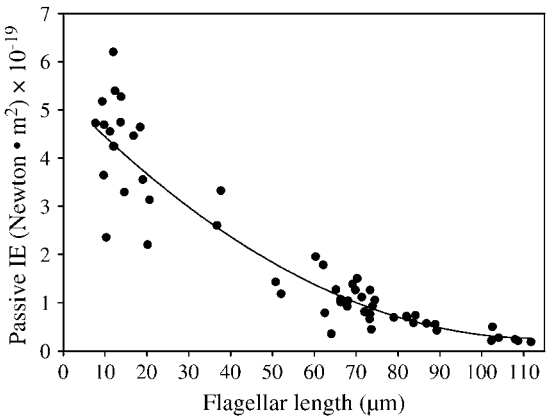

FIGURE 6 Stiffness of passive rat sperm flagella. Stiffness measurements of rat sperm flagella inhibited with 50 μM $NaVO_3$ in the presence of 0.1 mM ATP are plotted as a function of the position along the flagellum. A second order (quadratic) regression line is shown that gives a best fit to the data. The figure is reprinted in modified form from Schmitz-Lesich and Lindemann (10) with permission.

the elastic restoring force for cells with a small counterbend where the curvature is small. We corrected for the dead zone in the calculations of restoring torque in this study.

In the case of the counterbend, the torque that is doing the bending is generated by an internal restoring force that would normally be one component of the passive stiffness. If we consider a flagellum being bent by a microprobe, both the stiffness of the structures (i.e., the sheath, ODFs, and doublets) and the restoring force generated by the links between the doublets act as resistances to bending and oppose the action of the microprobe. This is analogous to a structure that engineers would call a ''sandwich beam'', consisting of two elastic plates separated by a shear web.

When such a structure is bent, resistance is contributed by both the elastic properties of the plates (E_1) and by the distension of the elastic web due to shear (E_2). The total resistance to bending is therefore a sum of $E_1 + E_2$ when the structure is bent by an externally imposed force. The counterbend beyond the microprobe is created by the restoring force acting between the doublets, in other words the elasticity of the web. The bending torque that develops from this restoring force acts in opposition to the stiffness of the structural components, so E_1 and E_2 become equal and opposite. This also means that the sum of the absolute values of the restoring torque and the structural resistance must approximately equal the passive stiffness as measured by an external microprobe (given that an equivalent bend is induced at the same flagellar position).

The relationship is only approximate because the second component, E_2, is shape dependent since it is derived from shear resistance. A stiffness measurement at a specified location on the flagellum requires the microprobe to contact the flagellum more distally than is the case when a counterbend is induced at the same flagellar position. Thus, the overall shape of the distal flagellum is not identical in the two cases. This factor would tend to increase the size of the contribution from the elastic web when the flagellum is forced into a bend because the imposed shear is usually greater in that configuration. This could have the effect of overestimating E_1 from the stiffness measurements. We examined the shear that was present in the stiffness measurement experiments by reviewing eight of the original images used for the stiffness determinations in the earlier study (10). The average shear was 20% greater in those experiments than the average for our 10 counterbend analyses. Consequently, our assertion that the effective structural stiffness in the counterbend is half of the total stiffness is a high-end estimate, and the true value may be as much as 20% less.

The curvature of the 20 μm of flagellum distal to the probe contact was found as described in Materials and Methods, and the stiffness value at this position along the flagellum was found from the regression line in Fig. 6. Half of the stiffness multiplied by the curvature (corrected for a dead zone of 1×10^4 radians/m) yielded the restoring torque responsible for the counterbend at this location.

The estimate of restoring torque found for each cell provided a way to find the tension on the doublets. The restoring torque is predominantly supplied by tension coming from doublets 1 and 5–6 acting across the distance found from Eq. 1 for the position of the curvature measurement. This distance is the effective diameter of the axoneme and is indicated as D_E in Fig. 4 *B*. A small contribution to the total restoring torque is provided by tension on doublets 2 and 4 on one side of the axoneme and 7 and 8 on the opposite side acting across the smaller lever arm given by Eq. 2. This smaller component of torque develops because a larger fraction of the total effective diameter D_E is between ODFs 2, 3, and 4 and 7, 8, and 9 (D_2 in Fig. 4 *B*) than is between the ODFs 9, 1, and 2 or 4, 5–6, and 7 (D_1 in Fig. 4 *B*). This means that not all of the tension developed by stretching the nexin links that connect to doublets 3 and 8 will be passed along to doublets 1 and 5–6. From the shears that are predicted by Eqs. 1 and 2, the ratio of torque contribution is 80% from ODFs 1 and 5–6 and 20% from the ODFs of the more central doublets. Therefore, to estimate the longitudinal force that is present on doublets 1 and 5–6, we took 80% of the restoring torque, found from the curvature and stiffness, and divided it by the 1 to 5–6 ODF spacing at the position of the measured curvature.

The shear between doublets 1 and 2 (and also between 1 and 9) will be half of the total shear, D_E, across the axoneme minus half of the shear between doublets 2 and 4 ($D_1 = D_E/2 - D_2$). Fig. 4 *B* may be helpful to visualize this relationship. Two sets of nexin links connect to doublet 1, one from doublet 9, and one from doublet 2. Therefore, if the longitudinal force is transmitted to doublet 1 via the nexin links, each of the two sets will supply half of the total. Assuming that all of the tension for the counterbend is supplied through the nexin, then the total force divided by the number of contributing nexin links will give us the force per nexin link. The number of contributing nexin links is two times the number of nexin links per unit length of doublet multiplied by the counterbend length distal to the curvature measurement point. The nexin link repeat interval is reported to be 96 nm.

The cells had values ranging from 1.1 pN to 3.3 pN average force per nexin in the counterbend region, as shown in Fig. 7. The interdoublet shear allows us to find the distension of the nexin along the counterbend utilizing a resting length of 30 nm and application of the Pythagorean Theorem. The same geometric relationship was also used to correct the tension acting along the nexin. The tension on the doublets was set equal to the vector component of force on the links acting along the doublet, using the averaged link geometry. The calculated average distension of the contributing nexin ranged from 16 nm to 209 nm, as shown in Fig. 7. From these values the nexin elasticity was found from the average distension of the nexin for each of the cells and ranged from 1.6 to 9.7×10^{-5} N/m. Three of the cells yielded values between 2 and 3 ($\times 10^{-5}$ N/m), which is an

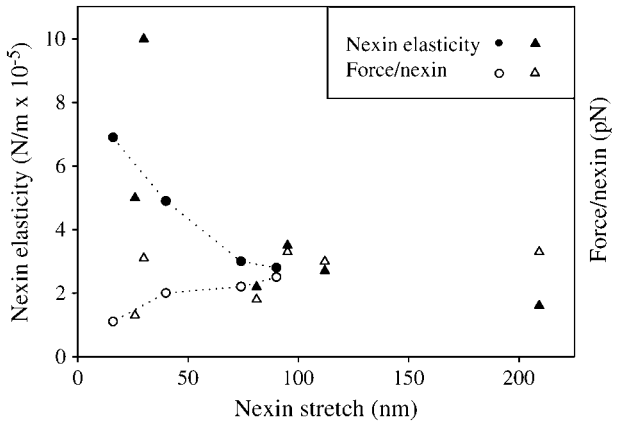

FIGURE 7 Properties of the interdoublet elastic resistance in the counterbend. The graph displays the results of calculating the interdoublet elastic resistance and restoring force for seven cells bent into counterbends of varied curvature (those listed in Table 1). We assumed that the nexin links are the most likely source of the resistance and have presented the data as elasticity and force per individual nexin link. The first six cells analyzed suggested that the apparent elasticity declines as the interdoublet sliding increases. The force increases with increased shear, but progressively less of an increase is seen as sliding displacement becomes larger. A seventh cell was analyzed at four positions (*circles* connected by *dashed lines*) to confirm that a similar relationship could be documented in a single cell.

excellent match to the 2×10^{-5} N/m nexin link elasticity value found by Yagi and Kamiya (6) for sea urchin sperm.

The result that was most surprising was that the nexin link elasticity was not constant, but decreased with increased distention of the nexin links, as seen in Fig. 7. It also did not increase as might be expected for an elastic polymer reaching its elastic limit. Fig. 7 shows that for the seven cells analyzed there appears to be an inverse relationship of apparent elasticity and distension. In addition, the force per nexin increased only slightly as distention is increased. These results combined with the apparently extreme stretch that the links must bear suggest that something different from Hooke's law type elasticity is acting at the linkers.

We noticed the unexpected relationship between increasing stretch and decreasing apparent elasticity after analyzing the first six independently bent cells listed in Table 1. We had some concern that the relationship might have been an accidental result of scatter due to the inclusion of cells with very different probe positions and different geometries at the point of measurement. The seventh cell listed in Table 1 was selected because it was recorded as a continuous sequence that allowed the counterbend to be analyzed at four different amounts of imposed bending. The probe position changed by only a small amount ($\sim$10 μm) during the sequence, whereas the induced interdoublet shear changed by almost a factor of 4. The results from this cell are connected by dashed lines in Fig. 7 to show the relationship that emerges from the same cell bent to different amounts of induced shear. The same general relationship in both apparent elasticity and force per nexin emerges from the multiple analyses on cell No. 7 as was suggested from the six independent cells. This is a positive confirmation that the reduction in the apparent interdoublet elasticity with increasing stretch is a real property of the counterbend and not based on cell to cell variation.

DISCUSSION

The mechanical properties exhibited by rat sperm flagella whose dynein are disabled with 50 μM $NaVO_3$ are interesting and complex. When these flagella are bent with a microprobe, the portion of the flagellum distal to the probe assumes a curved configuration in the direction opposite of the imposed bend. The magnitude of the ''counterbend'' curvature increases as the shear angle imposed on the flagellum by the microprobe is increased. This implies that internal interdoublet shear is responsible for counterbend formation. The counterbend is consistent with the sliding doublet model of flagellar mechanics but only if there are interdoublet linkages that resist shear and create an elastic restoring force. Additionally, the linkages would need to remember the zero-shear, or straight, configuration to which they return when released.

The most likely structures in the axoneme that could provide the restoring force that underlies the counterbend are the nexin links. When the dyneins have been disabled with vanadate, the remaining structures that bridge the doublets are the nexin links and the radial spokes. We have made the assumption in our analysis that the nexin links contribute all (or at least the majority) of the restoring force. This assumption is supported by the observation that the spokes are designed to accommodate interdoublet sliding by undergoing translocation, as has been demonstrated (30). Studies of the sliding disintegration of the axoneme that looked at the doublets after disintegration observed intact spokes present on the doublets (11,14,31). Consequentially, we must conclude that the presence of spokes does not prevent free sliding, and hence provides only limited resistance. Still, we must acknowledge that there may be a contribution to the counterbend effect from the spokes. Perhaps it will be possible to address the magnitude of this contribution in the future.

The first descriptions of the nexin links are coincident with the earliest electron microscope studies of flagellar structure (32–34). Subsequent studies have shown that the links repeat at the same interval as the radial spoke repeat pattern, $\sim$96 nm, and in register with spoke No. 1 (30,31,35). The nexin likely originate at or near the dynein regulatory complex on the inner surface of the A subtubule of each outer doublet and are ribbonlike in appearance (36). Despite what seems like a fairly extensive amount of specific observations on the nexin links, these structures are still something of a mystery and are controversial.

Quantitative analysis carried out in this study determined that interdoublet elasticity varies in the range of 1.6–10 $\times$

10^{-5} N/m per nexin link. The highest elasticity values are derived from the cases of least shear. This means that the elastic components (interdoublet linkages) do not exhibit linear Hooke's law behavior. Instead they show a high initial force threshold for distention and a much smaller increase in resistive force once distention is initiated. Theoretical analysis of the interdoublet shear resistance that has been developed in the past (37) assumed that the primary links exhibit a linear relationship of length to tension. That has also been the relationship adopted in modeling the flagellum (21,38). Our findings would suggest that this relationship must be reexamined in future models of the axoneme.

On first examination these results could be viewed as support for moveable linkages that reach a certain elastic limit, relocate, and then begin to stretch again. Such a scheme has some experimental support (7,35) and was successfully explored from a theoretical standpoint (39). An obvious merit of this interpretation is that it would yield a plateau of maximum resistance that our data imply is present. The challenge of this moveable element architecture is to conceive a mechanism for recoil to the original no-shear position when the external force is released. Recoil is not perfect in these passive flagella but results in far less residual curvature than would occur if the elastic linkers were required to establish new attachment positions.

Based on direct measurements, Minoura et al. (8) found steplike transitions in the longitudinal resistance to imposed sliding of doublets in the *Chlamydomonas* axoneme. From this they hypothesized that some of the interdoublet linkages may translocate, whereas others provide a constant elastic resistance. We see no evidence of a moveable elastic component in our high $NaVO_3$ observation conditions. It is possible that only the static linkages remain after utilizing our experimental conditions or that the interdoublet elastic connections are more permanent in large, structurally complex mammalian sperm like rat sperm.

One of the enduring puzzles of the flagellar axoneme is the nature of the nexin link. The Geometric Clutch model predicts that these linkages must contribute an elastic resistance that is important for the coordination of the flagellar beat (40–42). Unfortunately, a convincing protein or gene for the nexin link has yet to be identified. Thus far, the best protein candidate, called Rib 72 (43), is not a suitable protein to form a long elastic link.

A most intriguing possibility is suggested by recent work on structural proteins with Ig domains, such as filamin and titin (44,45). These proteins stretch when subjected to tension by unfolding several strands of a β-pleated sheet in structures called Ig folds, which open up in response to tension. When several Ig domains are linked together in series, the unfolding length can be dramatically large compared to the folded form of the molecule. The unfolding tension requirement has a steep initial phase followed by a saw-tooth of a gradually increasing tension requirement as each additional domain unfolds, since each opening of an Ig fold only requires an incrementally greater force than the previous one. This is nicely compatible with the weak force versus tension relationship that appears to be present in this study of rat sperm interdoublet linkages. Furthermore, these two elastic proteins associate with actin. For years it has been known that actin is a component of the axoneme (46) and is localized to the dynein regulatory complex (47). This complex is also thought to be the anchor point for the nexin linkages (36).

The first Ig domain of filamin reportedly needs nearly 40 pN of unfolding force to open (45). That is much higher than the force per nexin we determined. Titin, a large elastic protein of muscle, also has serial Ig domains, but much of the elasticity is provided by the uncoiling of PEVK regions, named for their richness in proline, glutamate, valine, and lysine residues. The combination of Ig domains and PEVK regions give titin the ability to maintain tension over a large variation of potential length, as required in the heart muscle (48). This property could be similarly useful in flagella where the range of interdoublet shear can be quite large and variable, depending on the beating pattern. Leake et al. (44) studied the elastic properties of titin and estimate that under physiological conditions the force per titin molecule, at an extension of 390 nm, is ~4 pN. This is remarkably similar to the force versus displacement we obtained here for the putative nexin links. Therefore, the basic mechanism that produces forces of the magnitude we are measuring is feasible and is described for at least one well-studied tension-bearing protein.

The fully extended lengths of 300 nm and 1200 nm for filamin and titin, respectively, are quite large, and both of these extensions are sufficient to accommodate most of the range of stretch we found for the interdoublet connections. At present, neither of these two proteins is reported in the ciliary/flagellar proteome (49). However, Ig domains, filamin repeats, and PEVK regions can be components of other proteins. These well-characterized sequences could help to identify a likely candidate for the nexin link protein from among the proteins in the flagellar proteome.

The authors thank Drs. Anne Hitt and John Reddan for many hours of useful discussion on the possible molecular implications of our results. Our thanks also go to Dr. Sheldon Gordon for suggesting the elastase experiment.

The project was supported by grant MCB-0110024 from the National Science Foundation.

REFERENCES

1. Satir, P. 1965. Studies on cilia. II. Examination of the distal region of the ciliary shaft and the role of the filaments in motility. *J. Cell Biol.* 26:805–834.
2. Satir, P. 1968. Studies on cilia. III. Further studies on the cilium tip and a ''sliding filament'' model of ciliary motility. *J. Cell Biol.* 39:77–94.
3. Summers, K., and I. R. Gibbons. 1971. Adenosine triphosphate-induced sliding of tubules in trypsin-treated flagella of sea urchin sperm. *Proc. Natl. Acad. Sci. USA.* 68:3092–3096.

4. Brokaw, C. J. 1999. Bending patterns of ATP-reactivated sea urchin sperm flagella following high salt extraction for removal of outer dynein arms. *Cell Motil. Cytoskeleton.* 42:125–133.

5. Linck, R. W. 1979. Advances in the ultrastructural analysis of the sperm flagellar axoneme. *In* The Spermatozoan. D. W. Fawcett and J. M. Bedford, editors. Urban and Schwarzenberg, Baltimore and Munich. 99–115.

6. Yagi, T., and R. Kamiya. 1995. Novel mode of hyper-oscillation in the paralyzed axoneme of a *Chlamydomonas* mutant lacking the central-pair microtubules. *Cell Motil. Cytoskeleton.* 31:207–214.

7. Bozkurt, H. H., and D. Woolley. 1993. Morphology of nexin links in relation to interdoublet sliding in the sperm flagellum. *Cell Motil. Cytoskeleton.* 24:109–118.

8. Minoura, I., T. Yagi, and R. Kamiya. 1999. Direct measurement of inter-doublet elasticity in flagellar axonemes. *Cell Struct. Funct.* 24:27–33.

9. Gibbons, I. R., and G. Mocz. 1991. Photocatalytic cleavage of proteins with vanadate and other transition metal complexes. *Methods Enzymol.* 196:428–442.

10. Schmitz-Lesich, K. A., and C. B. Lindemann. 2004. Direct measurement of the passive stiffness of rat sperm and implications to the mechanism of the calcium response. *Cell Motil. Cytoskeleton.* 59:169–179.

11. Shingyoji, C., and K. Takahashi. 1995. Cyclical bending movements induced locally by successive iontophoretic application of ATP to an elastase-treated flagellar axoneme. *J. Cell Sci.* 108:1359–1369.

12. Woolley, D. M. 1974. Freeze-substitution: a method for the rapid arrest and chemical fixation of spermatozoa. *J. Microsc.* 101:245–260.

13. Woolley, D. M. 2003. Motility of spermatozoa at surfaces. *Reproduction.* 126:259–270.

14. Lindemann, C. B., A. Orlando, and K. S. Kanous. 1992. The flagellar beat of rat sperm is organized by the interaction of two functionally distinct populations of dynein bridges with a stable central axonemal partition. *J. Cell Sci.* 102:249–260.

15. Calvin, H. I., and G. W. Cooper. 1979. A specific selenopolypeptide associated with the outer membrane of rat sperm mitochondria. *In* The Spermatozoan. D. W. Fawcett and J. M. Bedford, editors. Urban and Schwarzenberg, Baltimore and Munich. 135–140.

16. Olson, G. E., and R. W. Linck. 1977. Observations of the structural components of flagellar axonemes and central pair microtubules from rat sperm. *J. Ultrastruct. Res.* 61:21–43.

17. Gibbons, I. R., M. P. Cosson, J. A. Evans, B. Gibbons, B. Houck, K. H. Martinson, W. S. Sale, and W.-J. Y. Tang. 1978. Potent inhibition of dynein adenosine triphosphatase and of the motility of cilia and sperm flagella by vanadate. *Proc. Natl. Acad. Sci. USA.* 75:2220–2224.

18. Sale, W. S., and I. R. Gibbons. 1979. Study of the mechanism of vanadate inhibition of the dynein cross-bridge cycle in sea urchin sperm flagella. *J. Cell Biol.* 82:291–298.

19. Okuno, M. 1980. Inhibition and relaxation of sea urchin sperm flagella by vanadate. *J. Cell Biol.* 85:712–725.

20. Brokaw, C. J. 1971. Bend propagation by a sliding filament model for flagella. *J. Exp. Biol.* 55:289–304.

21. Brokaw, C. J. 1972. Computer simulation of flagellar movement. I. Demonstration of stable bend propagation and bend initiation by the sliding filament model. *Biophys. J.* 12:564–586.

22. Asai, D. J., and C. J. Brokaw. 1980. Effects of antibodies against tubulin on the movement of reactivated sea urchin sperm flagella. *J. Cell Biol.* 87:114–123.

23. Brokaw, C. J. 1980. Elastase digestion of demembranated sperm flagella. *Science.* 207:1365–1367.

24. Brokaw, C. J. 1991. Microtubule sliding in swimming sperm flagella: direct and indirect measurements on sea urchin and tunicate spermatozoa. *J. Cell Biol.* 114:1201–1215.

25. Gibbons, I. R. 1961. The relationship between the fine structure and direction of beat in gill cilia of a *lamellibranch mollusc*. *J. Biophys. Biochem. Cytol.*11:179–205.

26. Lindemann, C. B. 1996. Functional significance of the outer dense fibers of mammalian sperm examined by computer simulations with the Geometric Clutch model. *Cell Motil. Cytoskeleton.* 34:258–270.

27. Lindemann, C. B., and I. R. Gibbons. 1975. Adenosine triphosphate-induced motility and sliding of filaments in mammalian sperm extracted with Triton X-100. *J. Cell Biol.* 65:147–162.

28. Fawcett, D. W. 1975. The mammalian spermatozoan. *Dev. Biol.* 44: 394–436.

29. Vernon, G. G., and D. M. Woolley. 2002. Microtubule displacement at the tips of living flagella. *Cell Motil. Cytoskeleton.* 52:151–160.

30. Warner, F. D., and P. Satir. 1974. The structural basis of ciliary bend formation: radial spoke position changes accompanying microtubule sliding. *J. Cell Biol.* 63:35–63.

31. Witman, G. B., J. Plummer, and G. Sander. 1978. Chlamydomonas flagellar mutants lacking radial spokes and central tubules: structure, composition, and function of specific axonemal components. *J. Cell Biol.* 76:729–747.

32. Afzelius, B. A. 1959. Electron microscopy of the sperm tail. Results obtained with a new fixative. *J. Biophys. Biochem. Cytol.* 5:269–278.

33. Afzelius, B. A. 1961. The fine structure of the cilia from ctenophore swimming-plates. *J. Biophys. Biochem. Cytol.* 9:383–394.

34. Gibbons, I. R., and A. V. Grimstone. 1960. On flagellar structure in certain flagellates. *J. Biophys. Biochem. Cytol.* 7:697–716.

35. Warner, F. D. 1983. Organization of interdoublet links in *Tetrahymena* cilia. *Cell Motil.* 3:321–332.

36. Woolley, D. M. 1997. Studies on the eel sperm flagellum. 1. The structure of the inner dynein arm complex. *J. Cell Sci.* 110:85–94.

37. Hines, M., and J. J. Blum. 1978. Bend propagation in flagella. I. Derivation of equations of motion and their simulation. *Biophys. J.* 23:41–57.

38. Lindemann, C. B. 1994. A Geometric Clutch hypothesis to explain oscillations of the axoneme of cilia and flagella. *J. Theor. Biol.* 168: 175–189.

39. Cibert, C. 2001. Elastic extension and jump of the flagellar nexin links: a theoretical mechanical cycle. *Cell Motil. Cytoskeleton.* 49:161–175.

40. Lindemann, C. B. 1994. A model of flagellar and ciliary functioning which uses the forces transverse to the axoneme as the regulator of dynein activation. *Cell Motil. Cytoskeleton.* 29:141–154.

41. Lindemann, C. B., and K. S. Kanous. 1995. ''Geometric Clutch'' hypothesis of axonemal function: key issues and testable predictions. *Cell Motil. Cytoskeleton.* 31:1–8.

42. Lindemann, C. B., and K. S. Kanous. 1997. A model for flagellar motility. *Int. Rev. Cytol.* 173:1–72.

43. Ikeda, K., J. A. Brown, T. Yagi, J. M. Norrander, M. Hirono, E. Eccleston, R. Kamiya, and R. W. Linck. 2003. Rib72, a conserved protein associated with the ribbon compartment of flagellar A-microtubules and potentially involved in the linkage between outer doublet microtubules. *J. Biol. Chem.* 278:7725–7734.

44. Leake, M. C., D. Wilson, M. Gautel, and R. M. Simmons. 2004. The elasticity of single titin molecules using a two-bead optical tweezers assay. *Biophys. J.* 87:1112–1135.

45. Schwaiger, I., A. Kardinal, M. Schleicher, A. A. Noegel, and M. Rief. 2004. A mechanical unfolding intermediate in an actin-crosslinking protein. *Nat. Struct. Mol. Biol.* 11:81–85.

46. Piperno, G., K. Mead, and W. Shestak. 1992. The inner dynein arms I2 interact with a ''dynein regulatory complex'' in *Chlamydomonas* flagella. *J. Cell Biol.* 118:1455–1463.

47. LeDizet, M., and G. Piperno. 1995. The light chain p28 associates with a subset of inner dynein arm heavy chains in *Chlamydomonas* axonemes. *Mol. Biol. Cell.* 6:697–711.

48. Watanabe, K., P. Nair, D. Labeit, M. S. Z. Kellermayer, M. Greaser, S. Labeit, and H. Granzier. 2002. Molecular mechanics of cardiac titin's PEVK and N2B spring elements. *J. Biol. Chem.* 277:11549–11558.

49. Ostrowski, L. E., K. Blackburn, K. M. Radde, M. B. Moyer, D. M. Schlatzer, A. Moseley, and R. C. Boucher. 2002. A proteomic analysis of human cilia: identification of novel components. *Mol. Cell. Proteomics.* 1:451–465.